Insights into the linear and non-linear optical characteristics of substituted bi-naphthyl-2-pyrazolines

Houda El Karout, Chiraz Labassi, Karolina Waszkowska, Nicolas Fournier-Le Ray, Rafik Gatri, Fabienne Gauffre, Arnaud Fihey, Bouchta Sahraoui, Jean-Luc Fillaut

Insights into the linear and non-linear optical characteristics of substituted bi-naphthyl-2-pyrazolines

Houda El Karout[a],[b], Chiraz Labassi[c],[d], Karolina Waszkowska[a], Nicolas Fournier-Le Ray[c], Rafik Gatri[d], Fabienne Gauffre[c], Arnaud Fihey[c], Bouchta Sahraoui*[a], Jean-Luc Fillaut*[c].

[a] H. El Karout, K. Waszkowska, B. Sahraoui.
Univ Angers, LPHIA, SFR MATRIX, F-49000 Angers, France
[b] H. El Karout.
Univ Angers, CNRS, MOLTECH-ANJOU, SFR MATRIX, F-49000 Angers, France
[c] C. Labassi, N. Fournier-Le Ray, F. Gauffre, J.-L. Fillaut, A. Fihey.
Université de Rennes, Institut des Sciences Chimiques de Rennes CNRS UMR 6226, Rennes, France
[d] C. Labassi, R. Gatri.
Department of chemistry, Laboratoire de synthèse organique et hétérocyclique sélective-Evaluation d'activité biologique, LR17ES01, Université de Tunis El Manar

Corresponding authors: E-mail: jean-luc.fillaut@univ-rennes.fr, bouchta.sahraoui@univ-angers.fr

Supporting information for this article is given via a link at the end of the document.

Abstract

Donor/acceptor substitutions of a series of naphthyl bi-substituted 2-pyrazolines at accurate positions leads to large variations of their optical properties. An insightful discussion, supported by theoretical Density functional theory (DFT) calculations, is presented on how the intrinsic polarization of the 2-pyrazoline core influences dipole moment, charge transfer, and optical properties, with distinct patterns based on substituent attachment enhancing either second or third harmonic generation. In particular, this study highlights the importance of the juxtaposition of electron-releasing sub-units within small molecules for modulating their second and third-order susceptibilities in PMMA films. The DFT calculations corroborated these experimental findings, underscoring the importance of substituent effects, enriching our understanding and enabling the development of novel materials with customizable optical functions.

Graphical abstract

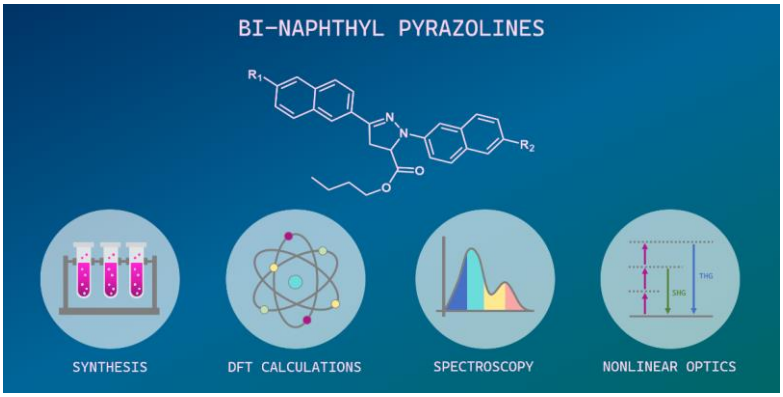

Donor/acceptor substituants in binaphthyl-2-pyrazolines significantly alter their optical properties, with DFT calculations that the arrangement of the electron-releasing units is key to modulating 2d- and 3rd-order susceptibilities in PMMA films.

Donor/acceptor substituants in binaphthyl-2-pyrazolines significantly alter their optical properties, with DFT calculations that the arrangement of the electron-releasing units is key to modulating 2d- and 3rd-order susceptibilities in PMMA films.

Donor/acceptor substitutions in binaphthyl-2-pyrazolines significantly modify their optical properties. DFT calculations confirm that the arrangement of electron-releasing units is crucial for modulating 2nd- and 3rd-order susceptibilities in PMMA films.

Keywords

Organic nonlinear optical materials
Binaphthyl 2-pyrazolines
Small π-conjugated organic molecules
DFT calculations
Second and third order nonlinear properties

Introduction

The development of nonlinear optical (NLO) molecules has attracted the spotlight of current research in view of applications in photonic technologies, such as multiphoton microscopy,[1] photodynamic therapy,[2] optical limiting,[3] multiphoton fabrication.[4] Among the classes of materials that have been investigated for NLO properties, organic materials received special attention because of their tuneable properties through structural modifications so that they can exhibit high nonlinearity and ultra-fast response. Key molecular features determining the structure of a highly active nonlinear chromophore are the extent of conjugation and the presence of charge transfer (π-donor and π-acceptor) groups to increase the charge transfer from the end(s) of the molecule to the centre.[5–7] Thus, researchers have developed numerous design strategies such as donor–acceptor–donor (D–A–D), acceptor–donor–acceptor (A–D–A) and donor–pi–donor (D–π–D) architectures. These conjugated organic molecules are also popular for their potential to provide solid-state organic materials characterized by large non-linear optical functions. Meanwhile, recent studies underline the benefits of developing small organic molecules with a π-conjugated system that consists of only a few multiple bonds, to access high quality nonlinear optical material.[8] These molecules possess distinct electronic properties that result from their delocalized electron density, allowing considerable flexibility in tuning their optical characteristics. The addition of donor and acceptor groups to these systems enhances their non-linear optical responses, enabling them to achieve high third-order non-linear optical polarizabilities. Considering that research in this area has the potential to reveal new opportunities for advanced optical devices, with a particular focus on the use of small organic compounds to create next-generation non-linear optical materials, we have synthesized a series of 1,3-naphthyl disubstituted 2-pyrazoline derivatives in which naphthyl groups have been connected to increase the conjugate length of the systems, while the introduction of peripheral donor and acceptor groups should enhance intramolecular delocalization and improve the NLO properties of the structures. 2-pyrazolines are small molecules that inspired chemists to carry out various structural variations in the ring to tune their optoelectronic properties, owing to their specific chemical structure in which electron donor and electron acceptor segments are joined together.[9–12] These segments are conjugated through the -N1-N2=C3- fragment of the 2-pyrazoline ring, which participates in the extension of internal charge transfer (ICT).

Materials and methods

Quartz tubes were used for the synthesis of 2-pyrazoline derivatives. Unless otherwise specified, reagents and solvents were purchased from commercial sources and used without further purification. The tetrazoles **T1-T7** (Scheme 1) were obtained using an adapted procedure of the Kakehi method.[13, 14] Column chromatography purifications were performed using 400-mesh silica gel with a particle size of 40-63 μm. Thin-layer chromatography (TLC) was carried out using silica gel 60 F254 plates, which were visualized under ultraviolet light. Spectroscopic measurements were performed using a UV-visible spectrophotometer JASCO®V 770 and a fluorimeter JASCO®FP 8300. NMR spectra of samples in $CDCl_3$ or CD_2Cl_2 were recorded on a Brucker AV 300 spectrometer. Chemical shifts are reported relative to tetramethylsilane (TMS).

The NLO characteristics of the compounds were investigated within host-guest systems, with poly(methyl methacrylate) (PMMA) serving as the matrix. Commercially available PMMA (Sigma Aldrich, Mw = 120,000 by GPC) was dissolved in dichloromethane (DCM) forming a concentration of

5.0 wt%. Subsequently, compound powders were prepared and mixed with a PMMA/DCM solution to achieve a 5.0 wt% concentration of the compounds in PMMA by weight, in dry mass. The resulting solutions were applied onto cleaned glass substrates using the spin-coating technique at 1300 rpm for 30 seconds, utilizing an SCS G3 Spin Coater. Film thickness was determined using a Veeco DEKTAK 3 profilometer.

The second and third harmonic generation (SHG/THG) intensities were measured using an ultrafast Nd:YAG laser (Ekspla, PL2250) operating at the wavelength of 1064 nm under the following parameters: frequency of 10 Hz, pulse duration of 30 ps, with the energy of the laser beam approximately 75 µJ. The SHG/THG assessments employed the rotational Maker fringe technique for both S-P and P-P polarized fundamental laser beams.[15, 16] This method involved focusing the laser beam onto the sample, positioned on a rotator, allowing adjustment of the incident beam angle from - 60° to + 60° around the normal axis. This facilitated the detection of the transmitted beam by the sample as a function of the angle of incidence. The SHG/THG signal was selectively collected using an interference filter at a wavelength of 532 nm or 355 nm, respectively, placed before the detectors.

Computational details

All Density Functional Theory (DFT) results presented here where were obtained with the Gaussian 16 software,[17] using the PBE0 functional[18] and a 6-311+G(d,p) basis set. This DFT method has been selected as the most suited to reproduce the experimental properties of the chromophores (see for comparison purposes Table S2 and Figure S16 for results obtained with a range-separated hybrid functional, CAM-B3LYP). Ground-state geometry optimizations were followed by frequency calculations to ensure the presence of positive only eigenvalues and thus the validity of the energy minimum. In all steps were included solvent effect (THF) through a Polarizable Continuum Model (PCM).[19] Absorption properties were obtained by computing the first 15 excited states, and emission energies by optimizing the geometry of the first excited state. The charge transfer characteristics of the excitations, namely distance of transfer (D_{CT}) and amount of charge transferred (Q_{CT}) have been computed using Ciofini's approach,[20] and the values are gathered in Table S3.

Results and Discussions

According to Scheme 1, the disubstituted 1,3-naphthyl 2-pyrazoline derivatives **P1-7** were prepared by means of a photoinduced cycloaddition of 2,5-dinaphthyl tetrazoles with n-butyl acrylates.[21] In this reaction, known as "nitrile-imine mediated tetrazole-ene cycloaddition" (NITEC), a nitrile-imine intermediate is formed which reacts in the presence of a dipolarophile,[22] in this case acrylates, to form a 2-pyrazoline. The disubstituted tetrazoles were obtained using a procedure adapted from the Kakehi method,[13, 14] which involves coupling a naphthyl-hydrazone and a naphthyl-diazonium salt. This approach makes it easy to modify the naphthyl units to be introduced into the 2-pyrazoline structure. The positions occupied by these naphthyl substituents in the final 2-pyrazoline structures are the positions 1 and 3 of the heterocycle (Scheme 1), which we have hereafter defined as C3 and N1, for the sake of clarity. The choice of naphthyl substituents was guided by the aim to extend the possibilities of electron delocalization within the final 2-pyrazolines and to be able to study the respective effects of electron donor and acceptor groups. We have limited this study to two types of substituents, MeO- and -CO_2Et, representative of electron-donating and electron-accepting units, whose relative positions with respect to the C3 or N1 2-pyrazolines atoms have been varied.

Synthesis and characterization of 2-pyrazolines P1-P7

A solution of tetrazole **T1-7** (around 1.2 to 1.4 mmol) in THF (30 mL) was degassed under argon for 20 min. Butyl acrylate (40 eq) was added to this solution. The mixture was irradiated for 3 hours in a *Rayonet Reactor*© with 16 x 21 W ampoules (Emission centered on 300 nm, in accordance with the absorption spectra of tetrazoles **T1-7** in THF). After 3 hours of irradiation, monitoring by thin-layer chromatography (TLC) indicated complete consumption of the starting tetrazoles. The solvent was removed by evaporation yielding a pale-yellow oil. Addition of pentane resulted in the formation of a precipitate, which was filtered, washed with pentane (20 mL). The 2-pyrazolines **P1-P7** were then purified by flash chromatography on silica gel, using heptane–diethyl ether (60:40 v/v) as the mobile phase, and dried under vacuum (Scheme 1).

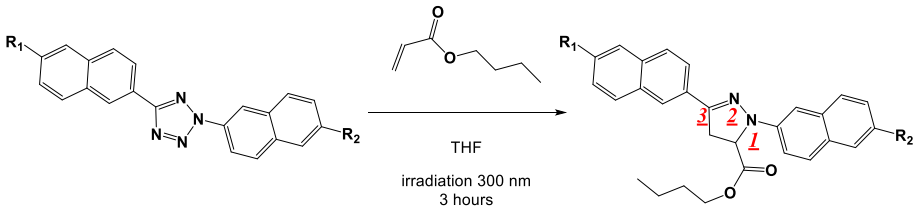

T1-T7

P1	R_1 = H	R_2 = H	69 %
P2	R_1 = OMe	R_2 = H	60 %
P3	R_1 = CO_2Et	R_2 = H	46 %
P4	R_1 = H	R_2 = OMe	59 %
P5	R_1 = H	R_2 = CO_2Et	72 %
P6	R_1 = CO_2Et	R_2 = OMe	57%
P7	R_1 = OMe	R_2 = CO_2Et	79%

Scheme 1: Synthesis of 2-pyrazolines **P1-P7.** The underlined numbers in italics correspond to the numbering of atoms in the 2-pyrazoline heterocycle. THF was chosen because binaphthyl tetrazoles are perfectly soluble in this solvent.

Butyl 1,3-di(naphthalen-2-yl)-4,5-dihydro-1H-pyrazole-5-carboxylate **P1** was obtained from **T1** (0.05 g, $0.141.10^{-3}$mol) and n-butyl acrylate (0.723 g, $5.64.10^{-3}$mol) with 69% yield (44.3 mg) as a yellow solid. ^{1}H NMR (300 MHz, $CDCl_3$) δ 8.18 (dd, J = 8.7, 1.7 Hz, 1H), 7.92 – 7.70 (m, 7H), 7.56 – 7.50 (m, 2H), 7.43 (td, *J* = 8.2, 6.8, 1.3 Hz, 1H), 7.28 (m, 2H), 7.22 (d, *J* = 2.3 Hz, 1H), 5.06 (dd, *J* = 12.6, 6.5 Hz, 1H), 4.20 (td, *J* = 6.7, 1.2 Hz, 2H), 3.85 (m, *J* = 12.6 Hz, 1H), 3.66 (m, *J* = 6.6 Hz, 1H), 1.57 (m, 2H), 1.26 (m, *J* = 15.5, 7.2 Hz, 2H), 0.82 (t, *J* = 7.3 Hz, 3H). ESIMS: $[M+Na]^+$ ($C_{28}H_{26}N_2O_2Na$) m/z Theoretical: 445.18865; m/z Found: 445.1891 (1 ppm); $[M+H]^+$ ($C_{28}H_{27}N_2O_2$) m/z Theoretical: 423.2067; m/z Found: 423.2061 (1 ppm).

Butyl 1-(6-methoxynaphthalen-2-yl)-3-(naphthalen-2-yl)-4,5-dihydro-1H-pyrazole-5-carboxylate **P2** was obtained from **T2** (0.051 g, $1.44.10^{-4}$mol) and butyl acrylate (0.746 g, $5.82.10^{-3}$mol) with 60% yield (39.5 mg) as a yellow amorphous solid. ^{1}H NMR (300 MHz, $CDCl_3$) δ 8.12 (dd, *J* = 8.7, 1.8 Hz, 1H), 7.85 – 7.67 (m, 7H), 7.40 (ddd, *J* = 8.2, 6.8, 1.4 Hz, 1H), 7.28 (d, *J* = 8.1 Hz, 1H), 7.21 – 7.13 (m, 3H), 5.01 (dd, *J* = 12.6, 6.5 Hz, 1H), 4.17 (td, *J* = 6.6, 1.3 Hz, 2H), 3.95 (s, 3H), 3.83 (dd, *J* = 17.0, 12.6 Hz, 1H), 3.58 (dd,

J = 17.0, 6.5 Hz, 1H), 1.38 – 1.14 (m, 4H), 0.79 (t, *J* = 7.3 Hz, 3H). ESIMS: $[M]^+$ ($C_{29}H_{28}N_2O_3$) m/z Theoretical: 452.20999; m/z Found: 452.2098 (1 ppm).

Butyl 1-(6-(ethoxycarbonyl)naphthalen-2-yl)-3-(naphthalen-2-yl)-4,5-dihydro-1H-pyrazole-5-carboxylate **P3** was obtained from **T3** (0.056 g, $1.42.10^{-4}$mol) and butyl acrylate (0.727 g, $5.67.10^{-3}$mol) with 46% yield (36 mg) as a yellow amorphous solid. ^{1}H NMR (300 MHz, $CDCl_3$) δ 8.62 – 8.57 (m, 1H), 8.22 (dd, *J* = 8.7, 1.7 Hz, 1H), 8.10 (dd, *J* = 8.6, 1.7 Hz, 1H), 7.97 (d, *J* = 8.7 Hz, 1H), 7.92 – 7.86 (m, 2H), 7.84 – 7.67 (m, 5H), 7.41 (ddd, *J* = 8.2, 6.8, 1.3 Hz, 1H), 7.33 – 7.26 (m, 1H), 7.20 (d, *J* = 2.3 Hz, 1H), 5.06 (dd, *J* = 12.7, 6.4 Hz, 1H), 4.46 (q, *J* = 7.1 Hz, 2H), 4.18 (td, *J* = 6.6, 1.7 Hz, 2H), 3.84 (dd, *J* = 17.0, 12.7 Hz, 1H), 3.60 (dd, *J* = 17.0, 6.4 Hz, 1H), 1.46 (t, *J* = 7.1 Hz, 3H), 1.36 – 1.13 (m, 4H), 0.79 (t, *J* = 7.3 Hz, 3H). ESIMS: $[M+Na]^+$ ($C_{31}H_{30}N_2O_4Na$) m/z Theoretical: 517.20978; m/z Found: 517.2096 (0 ppm); $[M+K]^+$ **(**$C_{31}H_{30}N_2O_4K$**)** m/z Theoretical: 533.18372; m/z Found: 533.1833 (1 ppm); $[M+H]^+$ **(**$C_{31}H_{31}N_2O_4$**)** m/z Theoretical: 495.22783; m/z Found: 495.2273 (1 ppm).

Butyl 3-(6-methoxynaphthalen-2-yl)-1-(naphthalen-2-yl)-4,5-dihydro-1H-pyrazole-5-carboxylate **P4** was obtained from **T4** (0.05 g, $1.42.10^{-4}$mol) and butyl acrylate (0.727 g, $5.67.10^{-3}$mol) with 59% yield (38.6 mg) as a yellow amorphous solid. ^{1}H NMR (300 MHz, CD_2Cl_2) δ 8.16 (dd, *J* = 8.6, 1.8 Hz, 1H), 7.95 – 7.82 (m, 4H), 7.76 – 7.59 (m, 3H), 7.57 – 7.46 (m, 2H), 7.20 (d, *J* = 2.2 Hz, 1H), 7.15 – 7.07 (m, 2H), 5.01 (dd, *J* = 12.6, 6.6 Hz, 1H), 4.19 (t, *J* = 6.6 Hz, 2H), 3.90 (s, 3H), 3.88 – 3.78 (m, 1H), 3.59 (dd, *J* = 17.1, 6.6 Hz, 1H), 1.65 – 1.56 (m, 2H), 1.39 – 1.22 (m, 2H), 0.85 (t, *J* = 7.3 Hz, 3H). ESIMS: $[M+Na]^+$ ($C_{29}H_{28}N_2O_3Na$) m/z Theoretical: 475.19921; m/z Found: 475.1991 (0 ppm); $[M+K]^+$ ($C_{29}H_{28}N_2O_3K$) m/z Theoretical: 475.19921; m/z Found: 475.1991 (0 ppm); $[M+H]^+$ ($C_{29}H_{29}N_2O_3$) m/z Theoretical: 453.21782; m/z Found: 453.21727 (1 ppm).

Butyl 3-(6-(ethoxycarbonyl)naphthalen-2-yl)-1-(naphthalen-2-yl)-4,5-dihydro-1H-pyrazole-5-carboxylate **P5** was obtained from **T5** (0.056 g, $1.42.10^{-4}$mol) and butyl acrylate (0.727g, $5.67.10^{-3}$mol) with 72% yield (50.3 mg) as a yellow amorphous solid. ^{1}H NMR (300 MHz, $CDCl_3$) δ 8.16 (dd, *J* = 8.6, 1.7 Hz, 1H), 8.00 (dd, *J* = 8.7, 1.7 Hz, 1H), 7.93 – 7.82 (m, 5H), 7.78 (dd, *J* = 9.0, 2.3 Hz, 1H), 7.71 (d, *J* = 8.8 Hz, 1H), 7.57 – 7.46 (m, 2H), 7.20 (s, 1H), 5.06 (dd, *J* = 12.5, 6.1 Hz, 1H), 4.43 (q, *J* = 7.1 Hz, 2H), 4.25 – 4.14 (m, 2H), 3.88 (dd, *J* = 17.1, 12.6 Hz, 1H), 3.63 (dd, *J* = 17.2, 6.1 Hz, 1H), 1.44 (t, *J* = 7.1 Hz, 3H), 1.31 – 1.23 (m, 4H), 0.79 (t, *J* = 7.4 Hz, 3H). ESIMS: $[M+Na]^+$ ($C_{31}H_{30}N_2O_4Na$) m/z Theoretical: 517.20978; m/z Found: 517.2084 (1 ppm); $[M+K]^+$ ($C_{31}H_{30}N_2O_4K$) m/z Theoretical: 533.18372; m/z Found: 533.1832 (1 ppm); $[M+H]^+$ ($C_{31}H_{31}N_2O_4Na$) m/z Theoretical: 495.22838 ; m/z Found: 495.2282 (1 ppm).

Butyl 3-(6-(ethoxycarbonyl)naphthalen-2-yl)-1-(6-methoxynaphthalen-2-yl)-4,5-dihydro-1H-pyrazole-5-carboxylate **P6** was obtained from **T6** (0.05 g, $0.117.10^{-3}$mol) and n-butyl acrylate (0.599 g, $4.68.10^{-3}$mol) with 79% yield (49 mg) as a yellow solid.^{1}H NMR (300 MHz, $CDCl_3$) δ 8.55 – 8.49 (m, 1H), 8.14 (dd, *J* = 8.7, 1.7 Hz, 1H), 8.01 (dd, *J* = 8.6, 1.7 Hz, 1H), 7.94 – 7.85 (m, 2H), 7.82 – 7.69 (m, 4H), 7.24 – 7.17 (m, 3H), 5.05 (dd, *J* = 12.5, 6.1 Hz, 1H), 4.45 (q, *J* = 7.1 Hz, 2H), 4.29 – 4.13 (m, 2H), 3.97 (s, 3H), 3.87 (dd, *J* = 17.1, 12.5 Hz, 1H), 3.63 (dd, *J* = 17.1, 6.1 Hz, 1H), 1.57 (m, 2H), 1.46 (t, *J* = 7.1 Hz, 3H), 1.34 – 1.19 (m, 2H), 0.81 (t, *J* = 7.4 Hz, 3H). ESIMS: $[M+Na]^+$ ($C_{32}H_{32}N_2O_5Na$) m/z Theoretical: 547.22034; m/z Found: 547.2210 (1 ppm); $[M+K]^+$ ($C_{32}H_{32}N_2O_5K$) m/z Theoretical: 563.19428; m/z Found: 563.1948 (1 ppm); $[M+H]^+$ ($C_{32}H_{33}N_2O_5$) m/z Theoretical: 525.2384; m/z Found: 525.2380 (1 ppm).

Butyl 1-(6-(ethoxycarbonyl)naphthalen-2-yl)-3-(6-methoxynaphthalen-2-yl)-4,5-dihydro-1H-pyrazole-5-carboxylate **P7** was obtained from **T7** (0.05 g, $0.117.10^{-3}$mol) and n-butyl acrylate (0.599 g, $4.68.10^{-3}$mol) with 57% yield (35 mg) as a yellow solid. ^{1}H NMR (300 MHz, $CDCl_3$) δ 8.62 (dd, *J* = 1.6 Hz, 1H), 8.24 (dd, *J* = 8.6, 1.6 Hz, 1H), 8.12 (dd, *J* = 8.6, 1.7 Hz, 1H), 7.98 (d, *J* = 8.7 Hz, 1H), 7.93 – 7.87 (m, 2H), 7.72 (d, *J* = 2.0 Hz, 2H), 7.68 – 7.61 (m, 1H), 7.22 (s, 1H), 7.13 (d, *J* = 8.0 Hz, 2H), 5.05 (dd, *J* = 12.6, 6.7 Hz, 1H), 4.48 (q, *J* = 7.1 Hz, 2H), 4.20 (td, *J* = 6.6, 1.7 Hz, 2H), 3.93 (s, 3H), 3.87 – 3.78 (m, 1H), 3.61 (dd, *J* = 17.0, 6.7 Hz, 1H), 1.56 (m, 2H), 1.48 (t, *J* = 7.1 Hz, 3H), 1.38 – 1.19 (m, 2H), 0.91 (t, *J* = 6.8 Hz, 3H). ESIMS: $[M+Na]^+$ ($C_{32}H_{32}N_2O_5Na$) m/z Theoretical: 547.22034; m/z Found: 547.2200 (1 ppm); $[M+K]^+$ ($C_{32}H_{32}N_2O_5K$) m/z Theoretical: 563.19428; m/z Found: 563.1936 (1 ppm); $[M+H]^+$ ($C_{32}H_{33}N_2O_5$) m/z Theoretical: 525.2384; m/z Found: 525.2392 (1 ppm).

Linear optical properties: absorption

Representative UV–visible absorption and fluorescence emission spectra of the 2-pyrazolines **P1-7** in tetrahydrofuran (THF) are shown in Fig. 1 and Fig. S1-7. The corresponding spectral data are listed in Table 1.

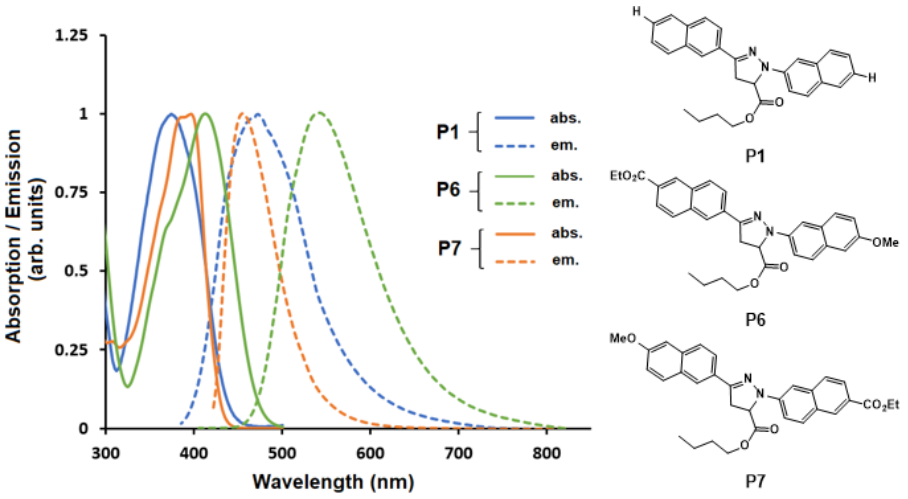

Fig. 1. Normalized UV–visible absorption and fluorescence emission spectra of 2-pyrazolines **P1**, **P6** and **P7** in THF ($C \approx 7.5\ 10^{-6}$ mol.L^{-1}).

P1-P7 exhibited strong absorption bands in the UV–vis range and more particularly in the region above 300 nm, which is what we will be focusing on. These bands correspond to the overlapping of several transitions, as evidenced by the presence of shoulders. Compared to the unsubstituted parent molecule **P1** (λ_{max} = 375 nm; ε_{max} = 23,650 $M^{-1}.cm^{-1}$), the incorporation of electron-donor (MeO-) and electron-acceptor ($EtCO_2$-) groups on the naphthyl substituents highlights several points. Whatever the position-1 (N-1) or position-3 (C-3) where the substituted naphthyl is linked to the 2-pyrazoline core, the effect of an electron-withdrawing group is more easily observed than that of its homologue with a

donor group. This is particularly noticeable when comparing **P2** (λ_{max} = 385 nm; ε_{max} = 44,605 $M^{-1}.cm^{-1}$) and **P3 (**λ_{max} = 405 nm; ε_{max} = 38,135 $M^{-1}.cm^{-1}$), but is also observed for **P4** and **P5** in a less marked way (Table 1). This observation is further supported by the fact that the effects of a donor or acceptor group, whatever the case may be, are always more significant if the substituted naphthyl is attached to the C3 (indicated as naphthyl-C3 thereafter) of the 2-pyrazoline ring (**P2** versus **P4**, λ_{max} = 376 nm; ε_{max} = 22,300 $M^{-1}.cm^{-1}$). Substituting a C3- or N1-naphthyl group with either a donor or an acceptor leads to a redshift, to a greater or lesser extent. The maximum redshift of wavelengths versus **P1** achieves $\Delta\lambda_{max}$ = 37 nm. It is obtained with **P6** (λ_{max} = 412 nm; ε_{max} = 104,075 M^{-1} cm^{-1}) for which it can be suggested that its UV-visible absorption properties result from the cumulative effect of the C3 acceptor and N1 donor groups, suggesting an efficient Intramolecular Charge Transfer (ICT) in this case. More generally, we assume that the different absorption peaks observed, as well as the values of the absorption coefficients, can be linked to an ICT character subject to the electronic effects and position of the electron-donor (MeO-) and electron-acceptor ($EtCO_2$-) groups, as rationalized after with (TD)-DFT calculations (see below).

Table 1. Photophysical properties of 2-pyrazoline derivatives in THF.

Compound	λ_{abs} [nm] (ε 10^4 M^{-1} cm^{-1})	λ_{flmax} / ($\lambda_{exc.}$) [nm]	Stokes shift [cm^{-1}]
P1	357 sh. (2.2515), 375 (2.3650)	473 / 385	5525
P2	388 sh. (4.4220), 385 (4.4605)	455 / 395	3340
P3	366 sh. (2.4135), 405 (3.8135)	506 / 415	4930
P4	376 (2.2300)	502 / 385	6680
P5	359 sh. (2.0050), 385 sh. (3.1250), 396 (3.1250)	454 / 405	3225
P6	370 (6.7136), 412 (10.4075)	541/420	5800
P7	360 (3.2856), 386 (4.6885), 396 (4.7216)	455/405	3275

Linear optical properties: Emission properties

All the 2-pyrazolines **P1-7** are emissive and show blue to green emission in THF with respect to substitution groups (Fig. 1 and Fig. S1-7). The emission maxima range from **P5** (λ_{flmax} = 454 nm) to **P6** (λ_{flmax} = 541 nm) (Table 1). In contrast to the absorption maxima, the 2-pyrazoline series can be easily classified into two distinct groups: **P2**, **P5** and **P7**, on the one side. **P3**, **P4** and **P6** on the other. The first group is characterized by a blueshift in emission relative to **P1** (λ_{flmax} = 473 nm). Interestingly, this situation corresponds to substitution by a C3 donor (**P2**; λ_{flmax} = 455 nm), a N1 acceptor (**P5**; λ_{flmax} = 454 nm) or a combination of both (**P7**; λ_{flmax} = 455 nm). Conversely, the 2-pyrazolines **P3**, **P4** and **P6** are characterized by an acceptor appended to naphthyl-C3 (**P3**; λ_{flmax} = 506 nm), or a donor to naphthyl-N1 (**P4**; λ_{flmax} = 502 nm), or a combination of both (**P6**; λ_{flmax} = 541 nm). These observations are suggestive of ICT from a donor part, located on the naphtyl-N1 and the 2-pyrazoline core, to an acceptor moiety, that approximately corresponds to the naphtyl-C3=N part of the 2-pyrazoline. Taking

in account only the emission wavelengths, we can suggest that this ICT increases in the order **P2**, **P5**, **P7** < **P4**, **P3** < **P6**.

Computational Studies

DFT based calculations (see computational details section were carried out to provide insights into the structure-properties relationship of these pyrazoline materials. The ground-state relaxed geometries of **P1-P7** all exhibit a planar π-conjugated backbone in the ground state. In Table 2 are presented the computed low-lying excitations for the different pyrazolines. In all cases the measured absorption band is attributed to an intense HOMO->LUMO $\pi-\pi^*$ electronic transition with a large oscillator strength, in a wavelength range (390-450 nm) in satisfying quantitative agreement with the experimental absorption throughout the series. The experimental trends are retrieved (vide infra) and the deviations of the computed absorption energy are system-dependent but remains in an acceptable range of 0.01 eV (for **P5**) up to 0.25 eV for **P4**. The computed emission energies are more accurately reproduced and deviate at most by 0.07 eV for **P7**. The frontier molecular orbitals of representative pyrazolines are shown in Fig. 2 (see the SI for the other pyrazolines).

Table 2. Computed ground state dipole moments, μ, and electronic gap, $\Delta E_{HO/LU,}$ in vacuum and in THF. Characteristics of the first excitation and de-excitation bands, computed in THF (see computational details).

Cpd	μ [D] in vacuum/THF	$\Delta E_{HO/LU}$ (eV) in vacuum/THF	λ_{abs} [nm] (*f*)	Transition description	λ_{em} [nm] (*f*)	Stokes shift [cm^{-1}]
P1	3.28/5.12	3.76/3.76	391 (1.26)	HOMO->LUMO	470 (1.46)	4299
P2	4.98/7.47	3.77/3.76	389 (1.39)	HOMO->LUMO	466 (1.66)	3617
P3	2.14/2.77	3.47/3.41	428 (1.26)	HOMO->LUMO	509 (1.48)	3718
P4	4.14/6.00	3.62/3.61	406 (1.18)	HOMO->LUMO	501 (1.28)	4670
P5	4.13/6.54	3.75/3.73	397 (1.68)	HOMO->LUMO	464 (1.97)	3637
P6	3.98/4.94	3.31/3.24	449 (1.17)	HOMO->LUMO	553 (1.29)	4188
P7	6.24/9.18	3.74/3.70	400 (1.81)	HOMO->LUMO	468 (2.19)	3633

In all 2-pyrazolines **P1-P7**, the HOMO electron density encompasses the central 2-pyrazoline ring, through the C3=N-N1 linkage, with a more pronounced density on the N1-naphthyl part, with the exception of 2-pyrazolines **P2** and **P7**, where the presence of a MeO- group on the naphthyl-C3 induces a more uniform distribution throughout these molecules, and of **P1**, which carries neither donor nor acceptor groups on its periphery, leading to the same observation. In the case of **P3**, which carries an acceptor group on the naphthyl-C3 unit, the electron density is more localized on the N1-naphthyl part. A distinction can be made between two series of 2-pyrazolines when considering the LUMO. In **P5** and **P7**, the electron densities are distributed throughout the molecules, whereas 2-pyrazolines **P1**-**P4** and **P6** present a very different situation: the LUMO is almost entirely localized on the naphthyl-C3 part. At this stage, it is interesting to compare **P6** and **P7**, which combine the effects of double substitutions by a donor (on Naphthyl-N1: **P6**; on C3-Naphthyl: **P7**) and an acceptor group (on C3-part:

P6; on N1-part: **P7**). For **P6**, HOMO localizes mainly on the central heterocyclic ring and on the N1-naphthyl part of this molecule, while LUMO resides on the central ring and on the naphthyl-C3 part. Thus, the extent of electron density transfer from HOMO to LUMO is very significant, which is consistent with an efficient ICT process during the excitation. Conversely, for **P7**, the electron density is univocally distributed throughout the molecule, at the different levels from HOMO-1 to LUMO+1, leading to a weaker electron density transfer.

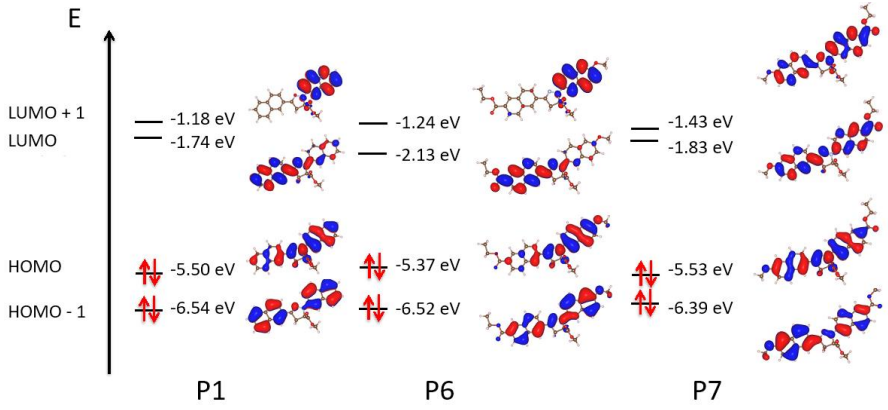

Fig. 2. Contour plots (iso-surface value = 0.02 au) and energy levels of the frontier molecular orbitals of 2-pyrazolines **P1**, **P6** and **P7** in THF (see computational details).

The calculated HOMO and LUMO energies (Table 2) range from −5.31 to −5.64 eV and −2.13 to −1.64 eV and are clearly dependent on the presence and localization of the electron donating or withdrawing units as can be seen from the energy level diagram in Fig. 2. The HOMO levels that reflect the electron releasing power of these 2-pyrazolines are more affected by substituent changes on the N1-naphthyl part than on the naphthyl-C3 part, whether by a donor group (**P4**: -5.31 eV, ΔE_{vsP1} = 0.19 eV; **P2**: - 5.40 eV, ΔE_{vsP1} = 0.10 eV) or an acceptor group (**P5**: -5.64 eV, ΔE_{vsP1} = -0.14 eV; **P3**: -5.57 eV, ΔE_{vsP1} = -0.07 eV). As expected, a donor group destabilizes the HOMO, unlike the introduction of an acceptor group. The effects of double substitutions are clearly more pronounced for **P6** (-5.37 eV, ΔE_{vsP1} = 0.13 eV) than for **P7** (-5.53 eV, ΔE_{vsP1} = -0.03 eV). Likewise, changes in these substituents affect the LUMO levels. The most noticeable effects are induced by the introduction of CO_2Et groups. For **P3**, where this electro-withdrawing group is positioned on the naphthyl-C3 moiety, the LUMO level is significantly stabilized (**P3**: -2.16 eV, ΔE_{vsP1} = -0.42 eV). **P6** presents a similar situation, given the double substitution where the electro-withdrawing group is positioned on the naphthyl-C3 moiety and the electron donating group on the N1-naphthyl one (**P6**: -2.13 eV, ΔE_{vsP1} = -0.39 eV). Obviously, the effects on HOMO and LUMO levels in these 2-pyrazolines cannot be considered completely as disconnected. In this respect, **P6** is revealing: its HOMO-LUMO gap (3.24 eV) is the smallest in the series studied, to be compared with **P1** (3.76 eV) or **P7** (3.70 eV). This observation mirrors the low-energy absorption and emission wavelengths observed and computed for this compound: the most red-shifted absorption of **P6** compared to the other dyes observed experimentally is retrieved, and attributed as a consequence of the electronic structure described above to the more pronounced CT character of the transition, followed by **P3** with a less important CT signature (see also the electronic density

difference in Figure S14). On the contrary **P2**/**P5**/**P7** exhibit a more delocalized π–π* transition, resulting in a blue-shifted transition compared to the other compounds. Table S3 presents the computed distance (D_{CT}) and amount of charge transferred (Q_{CT}) during excitation along the series, that correlates well with the above observations. **P5** and **P7** present for instance Q_{CT} values around 0.5 electron and D_{CT} below 2 Å, while **P6** exhibits the largest CT characteristics, with 0.8 electron transferred along almost 6 Å.

The extension of charge transfer in π-conjugated molecules can influence the magnitude of dipolar moments, with larger systems generally exhibiting stronger dipole moments compared to smaller ones, assuming other factors remain constant. However, in our study, **P7** emerges clearly in the series with the highest μ calculated values (6.24/9.18 D respectively in vacuum/THF), while **P6** display very similar values (3.98/4.94 D) to those of **P1** (3.28/5.12 D). These unexpected differences may be the result of the internal structuration of the 2-pyrazolines **P1-P7**. Indeed, they can be considered as the juxtaposition of sub-units whose character, in terms of donor or acceptor effect and respective positions, will influence the overall characteristics. In particular, the -C(3)=N(2)- group and the N(1) atom from the central heterocyclic ring probably display the properties of internal acceptor and donor moieties. In this respect, a comparison of the dipole moments of **P2** and **P3** reveals the importance of positioning a peripheral donor (**P2**) or electron withdrawing (**P3**) groups with respect to the -C(3)=N(2)- fragment: linking a donor group to naphthyl-C3 induces an increase of dipole moment (**P2**: $\Delta\mu_{vsP1}$= 1.7 D [vacuum]). Symmetrically, an acceptor group attached to the same position causes a weakening of the dipole moment (**P3**: $\Delta\mu_{vsP1}$= - 1.14 D). On the other hand, modifications by a donor or acceptor on the Naphthyl-N1 moiety result in fairly equivalent increases (**P4**: $\Delta\mu_{vsP1}$= 0.86 D; **P5**: $\Delta\mu_{vsP1}$= 0.85 D [vacuum]). Worthy to note, these effects seem to be cumulative for **P7** ($\Delta\mu_{vsP1}$= 2.96 D), but not for **P6** ($\Delta\mu_{vsP1}$= 0.7 D). It is therefore tempting to decompose the dipole moment of these molecules into a sum of the multiple dipole moments of the components of the 2-pyrazolines **P1-P7**, the sum of these individual dipole moments giving the total dipole moment of the molecule. This approach effectively approximates the dipole moments of **P6** and **P7**, these molecules being considered as "A-A'-D'-D" and "D-A'-D'-A" combinations (in this scheme, **P1** would be represented as A'-D', reflecting the intrinsic dipole moment common to all studied 2-pyrazolines).

After relaxation of the first excited state, only trifling geometry changes are observed and the chromophores remains planar. Computed emission wavelengths from this first π–π* exited state and Stokes shifts are presented in Table 2, showing a nice quantitative agreement with the experimental trends. The more blue-shifted emission of **P2**/**P5**/**P7** compared to **P1** is retrieved as well as the more red-shifted **P3**/**P4**/**P6** emission, with **P6** being the most red-shifted at 553 nm. Electronic density differences between the ground and the excited state illustrate these differences in Figure S15 and allow to link the evolution of the emission wavelengths to the CT vs. π delocalized character of the computed transition, mirroring the above discussion for the absorption. Same is true for the computed charge transfer characteristics D_{CT} and Q_{CT} *for* emission (Table S3) that follow the same evolution in the series as described above for absorption. From these calculations, the impact of the polar solvent (THF), modelled here as a dielectric continuum, is also clearly visible: the dipolar moments of the molecules are greatly increased and the absorption/emission wavelengths (see Table S1 for results obtained in vacuum) are red-shifted, as expected in such push-pull π-conjugated systems.

Nonlinear optical properties: Third Harmonic Generation

In Figure 3, Maker fringes illustrating the THG signals of host-guest thin films comprising **P1-P3** are displayed (Table 3). Supplementary figures for the compounds **P4-P7** are available in Fig. S8. All were analyzed in S-P input–output configuration of polarization (For S-polarization, the electric field vector of the laser light is perpendicular to the plane of incidence. For P-polarization, it is parallel to the plane of incidence). The third-order NLO susceptibility values were derived from the Maker fringes using the Kubodera–Kobayashi model (Eq. 1),[23] incorporating the absorption coefficient calculated from absorption spectra (refer to Fig. S9) at the 355 nm wavelength, which corresponds to THG, represented as follows:

$$\chi^{(3)} = \chi^{(3)}_{Silica}\left(\frac{2}{\pi}\right)\left(\frac{L^{coh}_{Silica}}{d}\right)\left(\frac{\frac{\alpha d}{2}}{1-exp\left(-\frac{\alpha d}{2}\right)}\right)\sqrt{\frac{I^{3\omega}}{I^{3\omega}_{Silica}}} \quad (1)$$

where $\chi^{(3)}_{Silica} = 2\cdot 10^{-22}\mathrm{m}^2.\mathrm{V}^{-2}$,[24] $L^{coh}_{Silica} = 6.7$ µm is the coherence length of reference material, α - linear absorption coefficient, d - the thickness of the sample and $I^{3\omega}$ and $I^{3\omega}_{Silica}$ are the THG intensities of the thin film and reference material, respectively.

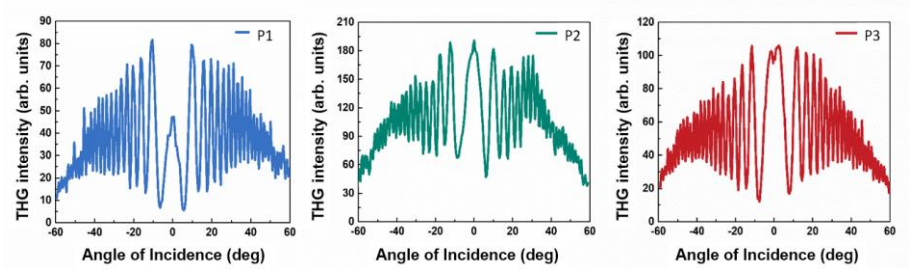

Fig. 3. The THG intensity of PMMA thin films of 2-pyrazolines **P1-P3**, as a function of the incident angle in S-P polarization.

When **P1** is adopted as reference model, the $\chi^{(3)}$of the other compounds increases consistently, with respect to this compound, with variations ranging from a minimum of +20% to a maximum of about +200%, as shown in Table 3. Notably, the smallest variations are observed in the monosubstituted compounds **P2**, featuring a MeO- group on Naphthyl-C3, and **P5**, in which an EtO_2C- group is bonded onto the N1-Naphthyl. Consistently, the ICT remains relatively subdued. The largest deviations occurred in **P4**, bearing a MeO- group on N1-Naphthyl, and **P3**, in which the EtO_2C- group is attached onto Naphthyl-C3. As a matter of fact, ICT is now much more enhanced and the deviations are almost equal to 100% each. Interestingly, these effects are cumulative in a way that the disubstituted systems, such as P6 and P7, exhibit significant variations compared to P1. Additionally, the positioning of each electron-donor or acceptor group in relation to the 2-pyrazoline core also has a significant impact on the response. Indeed, the structure **P7** displays a small increase of about +40% in its response with respect to **P1**, which corresponds overall to the sum of the variations of the monosubstituted compounds **P2** and **P5** (+20% each). Similarly, **P6** shows a remarkable $\chi^{(3)}$ augmentation (+ 200%), aligning with the combined contributions of the **P3** and **P4** (+100% each). These results are consistent with the approach of modulating the intramolecular charge transfer (ICT) in a molecule to optimize

first or higher order hyperpolarizabilities of conjugated organic molecules.[25] Further visualization of these third-order NLO susceptibility values is provided in Figure S10 in the SI.

Table 3. Values of the thickness (d), linear absorption coefficient (α_{355}), and third-order NLO susceptibility ($\chi^{(3)}$) of 2-pyrazoline derivatives thin films.

Compound	d [nm]	α_{355} [$\times 10^3$ cm^{-1}]	$\chi^{(3)}$ [$\times 10^{-22}\ m^2\ V^{-2}$]
P1	1023	7.73	10.54 ± 0.09
P2	1181	9.05	12.78 ± 0.11
P3	1230	3.40	21.73 ± 0.18
P4	1176	6.13	20.87 ± 0.18
P5	1268	5.87	12.55 ± 0.09
P6	986	4.48	30.79 ± 0.31
P7	1219	7.06	14.48 ± 0.12

Nonlinear optical properties: Second Harmonic Generation

SHG measurements were performed using two different polarization configurations of the fundamental laser beam: S-P and P-P (S-Vertical and P-Horizontal) (Table 4). These configurations, which represent different orientations of the laser beam's polarization, provide valuable insights into the complex dynamics of SHG phenomena. In Figure 4, we present typical Maker fringes, illustrating the SHG intensities of **P2-P4** samples in both polarization configurations: S-P and P-P (for other compounds, refer to Fig. S11).

To guarantee accuracy and consistency with theoretical expectations regarding symmetry, the corona poling method[26, 27] was applied to create a desired non-centrosymmetric orientation. This technique involves heating a polymer matrix containing the compounds to a temperature close to its glass transition temperature, followed by exposing them to a high voltage to induce dipole moment orientation. Specifically, we applied a voltage of 6 kV and set T_g = 100°C for the thin films, thereby enabling the alignment of molecular dipoles within the material.

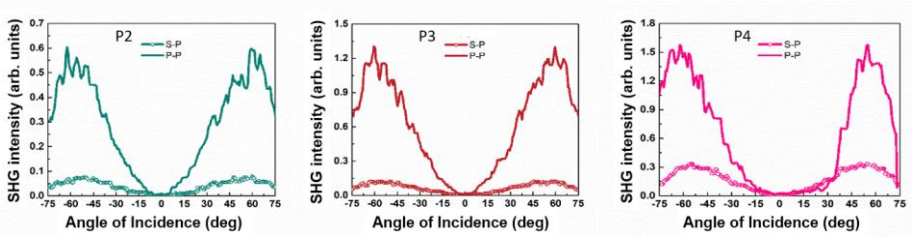

Fig 4. The SHG intensity of the 2-pyrazolines thin films **P2-P4**, as a function of the incident angle in two configurations S-P and S-P polarizations.

The determination of the second-order NLO susceptibility was obtained using the Lee model (Eq. 2).[28] The calculated values are summarized in Table 4.

$$\chi^{(2)} = \chi^{(2)}_{Quartz}\left(\frac{2}{\pi}\right)\left(\frac{L^{coh}_{Quartz}}{d}\right)\sqrt{\frac{I^{2\omega}}{I^{2\omega}_{Quartz}}} \quad (2)$$

where $\chi^{(2)}_{Quartz} = 1 \cdot 10^{-12}\,\mathrm{m.V^{-1}}$,[24] $L^{coh}_{Quartz} = 21\ \mu\mathrm{m}$ is the coherence length of the reference material, and $I^{2\omega}$ and $I^{2\omega}_{Quartz}$ are the SHG intensities of the thin film and reference material, respectively.

While the SHG signal shows a more significant enhancement for P-P polarization compared to S-P polarization, the observed $\chi^{(2)}$ values follow similar trends. A pivotal observation emerges when considering **P1** as a reference model: its lack of response aligns with expectations due to the absence of strongly electron-donating or attracting groups. Mono-substitution effects can therefore be monitored: the strongest effects are observed in the case of **P5**, following substitution of the Naphthyl-N1 moiety by an acceptor. Substituting this Naphthyl-N1 moiety with a donor (**P4**) gives more than twofold less (1.72 x 10^{-13} m.V^{-1} instead of 4.20 x 10^{-13} m.V^{-1}). The substitution effects of the Naphthyl-C3 part are even weaker (1.05 and 1.49 x 10^{-13} m.V^{-1} respectively).

The impact of substitutions is more pronounced in the disubstituted compounds. **P7**, featuring an EtO_2C- group on the N1-naphthyl and a MeO- group on the naphthyl-C3, for **P7**, exhibits the highest $\chi^{(2)}$ value ((8.32 ± 0.10) x 10^{-13} m.V^{-1} in P-P polarization) in the series. Intriguingly, **P6**, which internal structure favors ICT, displays a relatively modest $\chi^{(2)}$ value ((2.95 ± 0.04) x 10^{-13} m.V^{-1} in P-P polarization). The $\chi^{(2)}$ value observed for **P7** significantly surpasses what an additive effect resulting from the components of **P5** ((4.60 ± 0.06) x 10^{-13} m.V^{-1}) and **P2** ((1.05 ± 0.02) x 10^{-13} m.V^{-1}) would attain. A histogram presenting the second-order NLO susceptibility values is available in Fig. S12.

One possible explanation could be that the values we observed might not solely reflect intramolecular effects. Actually, previous researches [29, 30] have shown that molecular packing and orientation in polymer matrices can significantly impact the optical properties of dye-doped systems, emphasizing the role of intermolecular interactions, such as π-π stacking, in influencing their NLO behaviour. Thus, we assume that the ability of the **P1**-**P7** 2-pyrazolines to adjust a non-centrosymmetric polar ordering within the PMMA films and maintain this orientation within the materials could also contribute to the observed $\chi^{(2)}$ values. This can only be multifactorial. We assume that in the case of **P7**, two factors could contribute to a non-centrosymmetrical arrangement of the film: on the one hand, the overall dipole moment favors the responsiveness to electric field induction, and on the other, the juxtaposition of donor and acceptor subunits would approach D-A'-D'-A structuration, not particularly suitable for head-tail stacking. These two factors are lacking in **P6**: it's A-A'-D'-D internal structuration is likely to favor a centrosymmetric head-tail stacking, and its relatively weak overall dipole moment (3.98 D in vacuum) makes these molecules less amenable to field reorientation.

Table 4. Values of the thickness (d), and second-order NLO susceptibility ($\chi^{(2)}$) in S-P and P-P polarization of 2-pyrazoline derivatives thin films.

Compound	d [nm]	$\chi^{(2)}$ $[\times 10^{-13}$m.V$^{-1}]$	
		S-P	P-P
P1	1023	-	-
P2	1181	0.17 ± 0.02	1.05 ± 0.02
P3	1230	0.21 ± 0.02	1.49 ± 0.02
P4	1176	0.36 ± 0.01	1.72 ± 0.02
P5	1268	0.85 ± 0.01	4.60 ± 0.06
P6	986	0.45 ± 0.01	2.95 ± 0.04
P7	1219	1.40 ± 0.02	8.32 ± 0.10

These results confirm the relationship between molecular design, electronic structure, and optical response. Likewise, recent studies on the NLO properties of pyrazoline derivatives highlighted that variations in pyrazoline substituents strongly impact both $\chi^{(2)}$ and $\chi^{(3)}$.[31, 32] These studies are consistent with our findings, suggesting that systematic molecular modifications can enhance NLO properties for advanced applications.

Conclusion

A series of naphthyl bi-substituted 2-pyrazolines with various electron releasing parts was designed, synthesized, and investigated. Our focus was on the benefits of developing small organic molecules that consist of π-conjugated sub-units, to access high susceptibility nonlinear optical material. The straightforward synthetic method, through a photoinduced NITEC cycloaddition with binaphthyl tetrazoles, alternately substituted with donor or acceptor groups, allowed us to obtain such a series of bi-naphthyl 2-pyrazolines, in a fully controlled manner. These 2-pyrazolines exhibit optical properties, both linear and nonlinear, which were subsequently compared with each other.

The experimental linear optical (LO) and nonlinear optical (NLO) properties did not initially reveal a straightforward correlation with the overall chemical structures or the localization of the electron-donor or electron-acceptor units. Instead, contradictory results were observed, diverging from what might be expected based solely on conjugation extension or anticipated intramolecular charge transfers. This discrepancy is particularly notable when comparing the second and third-order susceptibilities of the disubstituted binaphthyl 2-pyrazolines **P6** and **P7**. While **P6**, with significant charge transfer, exhibits remarkable third-order response in a PMMA film, its second-order susceptibility is relatively moderate. Conversely, **P7** displays the opposite pattern. These differences can be explained in terms of the juxtaposition of subunits, with these molecules being considered as "A-A'-D'-D" and "D-A'-D'-A" combinations respectively. Such considerations offer an interesting approach that could be beneficial in the molecular design of small chromophores with desired NLO properties.

Importantly, our experimental results were confirmed using theoretical DFT calculations, which strengthens our findings. This comprehensive theoretical approach not only enhances our comprehension of how molecular structure influences the optical response but also provides a foundation for the development of new materials with tailored optical functions.

Acknowledgements

The authors would like to thank the ANR (ANR-19-CE06-0029-01), CNRS, the University of Tunis El Manar, and the Institut des Sciences Chimiques de Rennes for their support. Dr. B. Fabre for making the Rayonet® photoreactor available to us. The authors BS, KW, and HEK would like to acknowledge the partial funding provided by the EU IMAGE project for this research, supported by the EU Horizon 2020 research and innovation program under the Marie Skłodowska-Curie grant agreement No 778156.

Author contribution statement

All authors have participated in (a) conception and design, or analysis and interpretation of the data; (b) drafting the article or revising it critically for important intellectual content; and (c) approval of the final version. *Conceptualization:* KW, AF, BS, JLF; *Data curation:* HEK, CL, KW, NFLR, AF; *Formal analysis:* KW, FG, AF, BS, JLF; *Funding acquisition:* RG, BS; *Investigation:* HEK, CL, NFLR, AF; *Methodology:* NFLR, FG, AF, BS, JLF; *Supervision:* RG, FG, BS, JLF; *Validation:* AF, BS, JLF; *Writing – original draft:* AF, BS, JLF; *Writing – review & editing:* KW, FG, AF, BS, JLF.

Conflicts of Interest

The authors declare that they have no competing interests or personal relationships that could have influenced the work reported in this paper.

Supporting Information

Additional supporting information may be found online. It includes UV–visible absorption and fluorescence emission spectra of 2-pyrazolines **P1-P7**, UV-visible absorption spectra of **P1-P7** thin films, THG, SHG responses, third- and second-order NLO susceptibility values of **P1-P7** thin films, histograms presenting second- and third-order NLO susceptibility values, Contour plots (iso-surface value = 0.02 au) and energy levels of the frontier molecular orbitals levels of 2-pyrazolines **P2**-**P5** in THF.

REFERENCES

[1] Parodi, V.; Jacchetti, E.; Osellame, R.; Cerullo, G.; Polli, D.; Raimondi, M. T. Nonlinear Optical Microscopy: From Fundamentals to Applications in Live Bioimaging. *Front. Bioeng. Biotechnol.*, **2020**, *8*, 585363. https://doi.org/10.3389/fbioe.2020.585363.

[2] Bolze, F.; Jenni, S.; Sour, A.; Heitz, V. Molecular Photosensitisers for Two-Photon Photodynamic Therapy. *Chem. Commun.*, **2017**, *53* (96), 12857–12877. https://doi.org/10.1039/C7CC06133A.

[3] Gadhwal, R.; Devi, A. A Review on the Development of Optical Limiters from Homogeneous to Reflective 1-D Photonic Crystal Structures. *Opt. Laser Technol.*, **2021**, *141*, 107144. https://doi.org/10.1016/j.optlastec.2021.107144.

[4] Schwarz, C. M.; Grabill, C. N.; Digaum, J. L.; Williams, H. E.; Kuebler, S. M. Multiphoton Processing of Composite Materials and Functionalization of 3D Structures. In *Multiphoton Lithography*; Stampfl, J., Liska, R., Ovsianikov, A., Eds.; Wiley, 2016; pp 221–264. https://doi.org/10.1002/9783527682676.ch9.
[5] Andraud, C.; Fortrie, R.; Barsu, C.; Stéphan, O.; Chermette, H.; Baldeck, P. L. Excitonically Coupled Oligomers and Dendrimers for Two-Photon Absorption. In *Photoresponsive Polymers II*; Springer, 2008; pp 149–203.
[6] Liu, Z. J.; Chen, T.; Liu, B.; Huang, Z. L.; Huang, T.; Li, S. Y.; Xu, Y. X.; Qin, J. G. Two-Photon Absorption of a Series of V-Shape Molecules: The Influence of Acceptor's Strength on Two-Photon Absorption in a Noncentrosymmetric D-Pi-A-Pi-D System. *J. Mater. Chem.*, **2007**, *17*, 4685–4689. https://doi.org/10.1039/b707909e.
[7] Mongin, O.; Porrès, L.; Charlot, M.; Katan, C.; Blanchard-Desce, M. Synthesis, Fluorescence, and Two-Photon Absorption of a Series of Elongated Rodlike and Banana-Shaped Quadrupolar Fluorophores: A Comprehensive Study of Structure–Property Relationships. *Chem. - Eur. J.*, **2007**, *13* (5), 1481–1498. https://doi.org/10.1002/chem.200600689.
[8] Biaggio, I. The Appeal of Small Molecules for Practical Nonlinear Optics. *Chem. – Eur. J.*, **2022**, *28* (6), e202103168. https://doi.org/10.1002/chem.202103168.
[9] Varghese, B.; Al-Busafi, S. N.; Suliman, F. O.; Al-Kindy, S. M. Z. Unveiling a Versatile Heterocycle: Pyrazoline – a Review. *RSC Adv*, **2017**, *7* (74), 46999–47016. https://doi.org/10.1039/C7RA08939B.
[10] Haupa, K. A.; Szukalski, A.; Myśliwiec, J. Low-Molecular Push–Pull Pyrazoline Derivatives: Solvatochromic Effect and Theoretical Insights into Dye-Based Molecular Engineering. *J. Phys. Chem. A*, **2018**, *122* (39), 7808–7818. https://doi.org/10.1021/acs.jpca.8b04814.
[11] Uchacz, T.; Maroń, A. M.; Szlachcic, P.; Danel, A.; Pokladko-Kowar, M.; Gondek, E.; Kolek, P.; Zapotoczny, S.; Stadnicka, K. M. Photoinduced Charge Transfer in Push-Pull Pyrazoline-Based Chromophores – Relationship between Molecular Structure and Photophysical, Photovoltaic Properties. *Spectrochim. Acta. A. Mol. Biomol. Spectrosc.*, **2023**, *296*, 122643. https://doi.org/10.1016/j.saa.2023.122643.
[12] Karuppusamy, A.; Kannan, P. Effect of Substitution on Pyrazoline Based Donor-Acceptor Molecules as Luminescent and Their Electrochemical Properties. *Chem. Phys. Lett.*, **2020**, *745*, 137241. https://doi.org/10.1016/j.cplett.2020.137241.
[13] Ito, S.; Tanaka, Y.; Kakehi, A. Synthesis of 2,5-Diaryltetrazoles from *N* -Phenylsulfonylbenzhydrazidoyl Chlorides and Arylhydrazines. *Bull. Chem. Soc. Jpn.*, **1976**, *49* (3), 762–766. https://doi.org/10.1246/bcsj.49.762.
[14] Fournier-Le Ray, N.; Joly, N.; Fillaut, J.-L. Optimising the Synthesis of 2,5-Diaryltetrazoles: The Decisive Choice of the Reaction Solvent. *Tetrahedron*, **2023**, *143*, 133560. https://doi.org/10.1016/j.tet.2023.133560.
[15] El Karout, H.; Shchur, Y.; Andrushchak, A.; Sahraoui, B.; Wielgosz, R.; Kityk, O.; Jędryka, J.; Slyvka, Y.; Kityk, A. V. Second Harmonic Generation on Crystalline Organic Nanoclusters under Extreme Nanoconfinement in Functionalized Silica–Benzil Composites. *Sci. Rep.*, **2023**, *13* (1), 9943. https://doi.org/10.1038/s41598-023-37147-4.
[16] Marjanowska, A.; El Karout, H.; Guichaoua, D.; Sahraoui, B.; Płóciennik, P.; Zawadzka, A. Topography and Nonlinear Optical Properties of Thin Films Containing Iodide-Based Hybrid Perovskites. *Nanomaterials*, **2023**, *14* (1), 50. https://doi.org/10.3390/nano14010050.
[17] Frisch, M. J.; Trucks, G. W.; Schlegel, H. B.; Scuseria, G. E.; Robb, M. A.; Cheeseman, J. R.; Scalmani, G.; Barone, V.; Petersson, G. A.; Nakatsuji, H. Gaussian 16, Revision A. 03, Gaussian, Inc, Wallingford, CtT. **2016**.
[18] Adamo, C.; Barone, V. Toward Reliable Density Functional Methods without Adjustable Parameters: The PBE0 Model. *J. Chem. Phys.*, **1999**, *110* (13), 6158–6170. https://doi.org/10.1063/1.478522.

[19] Scalmani, G.; Frisch, M. J. Continuous Surface Charge Polarizable Continuum Models of Solvation. I. General Formalism. *J. Chem. Phys.*, **2010**, *132* (11), 114110. https://doi.org/10.1063/1.3359469.
[20] Le Bahers, T.; Adamo, C.; Ciofini, I. A Qualitative Index of Spatial Extent in Charge-Transfer Excitations. *J. Chem. Theory Comput.*, **2011**, *7* (8), 2498–2506. https://doi.org/10.1021/ct200308m.
[21] Kumar, G. S.; Lin, Q. Light-Triggered Click Chemistry. *Chem. Rev.*, **2021**, *121* (12), 6991–7031. https://doi.org/10.1021/acs.chemrev.0c00799.
[22] Pirota, V.; Benassi, A.; Doria, F. Lights on 2,5-Diaryl Tetrazoles: Applications and Limits of a Versatile Photoclick Reaction. *Photochem. Photobiol. Sci.*, **2022**, *21* (5), 879–898. https://doi.org/10.1007/s43630-022-00173-8.
[23] Kubodera, K.; Kobayashi, H. Determination of Third-Order Nonlinear Optical Susceptibilities for Organic Materials by Third-Harmonic Generation. *Mol. Cryst. Liq. Cryst. Inc. Nonlinear Opt.*, **1990**, *182* (1), 103–113. https://doi.org/10.1080/00268949008047792.
[24] Kajzar, F.; Okada-Shudo, Y.; Meritt, C.; Kafafi, Z. Second- and Third-Order Non-Linear Optical Properties of Multilayered Structures and Composites of C60 with Electron Donors. *Synth. Met.*, **2001**, *117* (1–3), 189–193. https://doi.org/10.1016/S0379-6779(00)00498-7.
[25] Samanta, P. K.; Misra, R. Intramolecular Charge Transfer for Optical Applications. *J. Appl. Phys.*, **2023**, *133* (2), 020901. https://doi.org/10.1063/5.0131426.
[26] Sahraoui, B.; Luc, J.; Meghea, A.; Czaplicki, R.; Fillaut, J. L.; Migalska-Zalas, A. Nonlinear Optics and Surface Relief Gratings in Alkynyl-Ruthenium Complexes. *J. Opt. -Pure Appl. Opt.*, **2009**, *11* (2). https://doi.org/10.1088/1464-4258/11/2/024005.
[27] Liu, J.; Ouyang, C.; Huo, F.; He, W.; Cao, A. Progress in the Enhancement of Electro-Optic Coefficients and Orientation Stability for Organic Second-Order Nonlinear Optical Materials. *Dyes Pigments*, **2020**, *181*, 108509. https://doi.org/10.1016/j.dyepig.2020.108509.
[28] Lee, G. J.; Cha, S. W.; Jeon, S. J.; Jin, J. I.; Yoon, J. S. Second-Order Nonlinear Optical Properties of Unpoled Bent Molecules in Powder and in Vacuum-Deposited Film. *J. Korean Phys. Soc.*, **2001**, *39* (5), 912–925.
[29] El Karout, H.; Özkonstanyan, A.; Sentürk, E.; Eran, B. B.; Taboukhat, S.; Zawadzka, A.; Szukalski, A.; El-Ghayoury, A.; Akdas-Kılıç, H.; Sahraoui, B. Innovative Triazine-Core Octupolar Chromophores: Unlocking New Frontiers in Nonlinear Optics. *J. Mater. Chem. C*, **2024**, *12* (30), 11458–11473. https://doi.org/10.1039/D4TC01975J.
[30] Jeong, M. -Y.; Kim, H. M.; Jeon, S. -J.; Brasselet, S.; Cho, B. R. Octupolar Films with Significant Second-Harmonic Generation. *Adv. Mater.*, **2007**, *19* (16), 2107–2111. https://doi.org/10.1002/adma.200700414.
[31] Papagiannouli, I.; Szukalski, A.; Iliopoulos, K.; Mysliwiec, J.; Couris, S.; Sahraoui, B. Pyrazoline Derivatives with a Tailored Third Order Nonlinear Optical Response. *RSC Adv.*, **2015**, *5* (60), 48363–48367. https://doi.org/10.1039/C5RA05912G.
[32] Szukalski, A.; Sahraoui, B.; Kulyk, B.; Lazar, C. A.; Manea, A. M.; Mysliwiec, J. Chemical Structure versus Second-Order Nonlinear Optical Response of the Push–Pull Type Pyrazoline-Based Chromophores. *RSC Adv.*, **2017**, *7* (16), 9941–9947. https://doi.org/10.1039/C6RA26781E.